


Singlet, triplet, and pair density wave superconductivity in the doped triangular-lattice moiré system

Feng Chen and D. N. Sheng

Phys. Rev. B **108**, L201110 — Published 13 November 2023

DOI: 10.1103/PhysRevB.108.L201110

Singlet, Triplet and Pair Density Wave Superconductivity in the Doped Triangular-Lattice Moiré System

Feng Chen and D. N. Sheng
Department of Physics and Astronomy, California State University, Northridge, California 91330, USA
(Dated: October 13, 2023)

Recent experimental progress has established the twisted bilayer transition metal dichalcogenide (TMD) as a highly tunable platform for studying many-body physics. Particularly, the homobilayer TMDs under displacement field are believed to be described by a generalized triangular-lattice Hubbard model with a spin-dependent hopping phase θ. To explore the effects of θ on the system, we perform density matrix renormalization group calculations for the relevant triangular lattice t-J model. By changing θ at small hole doping, we obtain a region of quasi-long-range superconducting order coexisting with charge and spin density wave within $0 < \theta < \pi/3$. The superconductivity is composed of a dominant spin singlet d-wave and a subdominant triplet p-wave pairing. Intriguingly, the $S_z = \pm 1$ triplet pairing components feature pair density waves. In addition, we find a region of triplet superconductivity coexisting with charge density wave and ferromagnetism within $\pi/3 < \theta < 2\pi/3$, which is related to the former phase at smaller θ by a combined operation of spin-flip and gauge transformation. Our findings provide insights and directions for experimental search for exotic superconductivity in twisted TMD systems.

Introduction.—Moiré bilayer systems have attracted great attention over the last few years due to their high tunability and capacity to host a wealth of exotic states of matter [1–3]. Since the discovery of superconductivity (SC) and Mott insulating phase in magic-angle twisted bilayer graphene (TBG) [4, 5], other Moiré systems have been realized and are under active studies [6, 7], including twisted bilayer transition metal dichalcogenides (TMDs) [8–17]. Compared to TBG, twisted bilayer TMDs have the advantages of accommodating flat Moiré bands over a much wider range of twist angles and fewer low-energy degrees of freedom, allowing for a simpler lattice model description [18–20]. Strong correlation effects such as correlated insulating phase [21], metal-insulator transition [22, 23], stripe phase [24] and quantum anomalous Hall effect [25] have recently been observed in these systems.

Twisted TMD bilayers can be classified into hetero- and homo-bilayers according to whether the two layers are made of the same or different materials. The low-energy electronic degrees of freedom in the former are believed to be described by a generalized triangular-lattice Hubbard model with pseudo-spin SU(2) rotation symmetry [18, 26], whereas in the latter the spin SU(2) symmetry is broken into U(1) by a vertical displacement field due to spin-valley locking and inversion symmetry breaking, and consequently the electron hopping acquires a spin-dependent phase θ [16, 19, 20, 27]. Note that the standard Hubbard and t-J models on triangular lattices, i.e. $\theta = 0$, have exhibited a rich phenomenology enhanced by further-neighbor couplings due to the complex interplay between geometric frustration, quantum fluctuations and hole dynamics [28–39]. The hopping phase θ is shown to be widely tunable by the displacement field and thus may serve as a novel control knob of the many-body ground states of twisted TMD homobilayers. The magnetic and superconducting phases under the variation of both carrier density and θ of the U(1) Hubbard model and/or its closely related t-J model (for strong Hubbard U limit) at/near half-filling have been explored through mean-field calculations, renormalization group analysis, quantum cluster methods and Gutzwiller approximation [20, 40–45]. However, these methods generally are not accurate in treating the strong electronic correlations present in the model [46]. Here we implement density matrix renormalization group (DMRG) [47] to accurately capture the ground states on quasi-1D few-leg cylinders, and thus reveal the different ordering tendencies at play and gain some insights into the physics at the 2D limit [48, 49]. Particularly, DMRG has been applied onto a three-leg cylindrical Moiré Hubbard model but only weak SC correlations were observed [50]. The effective spin-model derived at strong U and half-filling limit was also considered for exploring quantum spin liquid [51].

In this work we study SC of the lightly doped triangular lattice U(1) Moiré t-J model on a four-leg cylinder through DMRG calculations. By varying θ in the region of $(0, \frac{2\pi}{3})$, we identify two conjugated superconducting phases as shown in Fig. 1(b): (i) Mixed spin singlet d-wave and triplet p-wave SC coexisting with spin, charge and pair density waves (PDW); (ii) Ferromagnetic triplet p-wave SC coexisting with charge density wave (CDW). These two phases are related by a combined operation of spin flip and local gauge transformation, up to a change of the boundary condition. Their pairing correlations decay algebraically with the Luttinger exponents smaller or around two, demonstrating a robust quasi-long-range SC order [52, 53]. Particularly, distinct from other SC phases on the triangular-lattice t-J model [29, 31, 54], PDW is a novel SC state where Cooper pairs carry finite center-of-mass momentum [55], which are not commonly realized in microscopic models [56–65]. The plethora of interesting phases found in our calculations could motivate future experimental endeavour in search of novel SC in twisted TMD homobilayers.

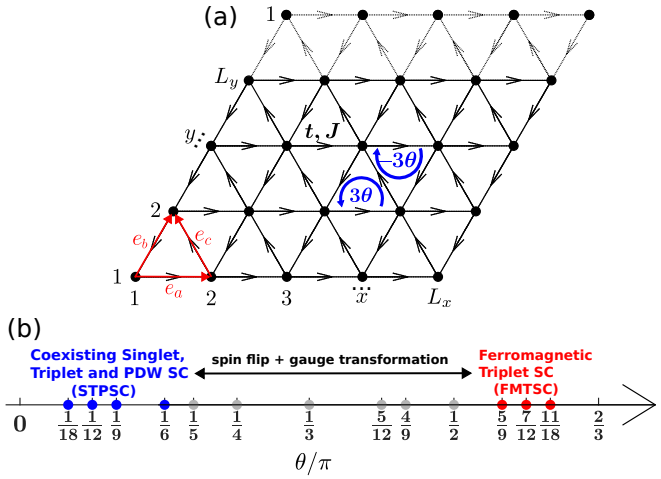

FIG. 1. (a) Schematic illustration of the Moiré t-J model on a triangular lattice with nearest-neighbor electron hopping (t) and spin exchange (J). The arrow on each bond is pointed from site i to j in the Hamiltonian Eq. 1. It denotes the directional dependence of the hopping phase.The first and last rows are identified together due to the periodic boundary condition. (b) Quantum phase diagram under the variation θ for a width-four cylinder. Gray dots denote θs where no clear signature of SC is observed [66].

Model and Method.— The Moiré t-J model is defined as

$$\hat{H} = -t \sum_{\langle ij\rangle,\sigma=\pm} (e^{-i\sigma\theta}\hat{c}^\dagger_{i\sigma}\hat{c}_{j\sigma} + \text{h.c.}) + J\sum_{\langle ij\rangle}(\hat{S}^z_i\hat{S}^z_j + \frac{1}{2}e^{-2i\theta}\hat{S}^+_i\hat{S}^-_j + \frac{1}{2}e^{2i\theta}\hat{S}^-_i\hat{S}^+_j - \frac{1}{4}\hat{n}_i\hat{n}_j), \quad (1)$$

where $\sigma = \pm$ represents spin up/down, $c^\dagger_{i\sigma}$ and $c_{i\sigma}$ are the creation and annihilation operators for the electron with spin σ at the site i, $\langle ij\rangle$ denote nearest neighbors whose locations satisfy $\boldsymbol{r}_j - \boldsymbol{r}_i \in \{\boldsymbol{e}_a, -\boldsymbol{e}_b, \boldsymbol{e}_c\}$ (see Fig. 1(a)), $\hat{S}^z_i, \hat{S}^+_i, \hat{S}^-_i$ are the spin-$\frac{1}{2}$ $\hat{z}$ component, raising and lowering operators at site i respectively, and $\hat{n}_i = \sum_\sigma \hat{c}^\dagger_{i\sigma}\hat{c}_{i\sigma}$ is the electron number operator. Double occupancy is prohibited. The hopping phase θ produces a flux of $\pm 3\theta$ at each triangular plaquette, and a gauge transformation connects two models differing in the fluxes by 2π. We therefore focus on the region of $0 < \theta < 2\pi/3$. In the present study, we set the hole doping level $\delta = 1/12$, and choose $J = 1$ and $t = 3$, corresponding to a realistic situation of $U/t = 12$ [20].

To obtain the ground state, we employ DMRG simulation with U(1)×U(1) symmetry corresponding to charge and spin conservation on a cylindrical system with periodic boundary condition (PBC) along the circumferential ($\boldsymbol{e}_b$ or y-) direction and open boundary condition along the axial ($\boldsymbol{e}_a$ or x-) direction. The number of lattice sites is given by $N = L_x \times L_y$, where L_x and L_y are the number of sites along x- and y-direction respectively and are set as $L_y = 4$ and $L_x = 36$ in the main text. The corresponding geometry is called YCL_y [67]. The doping level is defined by $\delta = 1 - N_e/N$ and we consider the zero total spin-z sector: $\sum_i \hat{S}^z_i = 0$, which hosts the ground state as verified in Sec. A of the supplemental materials (SM) [66]. In DMRG, the number of Schmidt states kept for representing the reduced density matrix on either side of the system under bipartition is called "bond dimension" M[47] The calculations improve with the increase of M and become exact for a sufficiently large M.

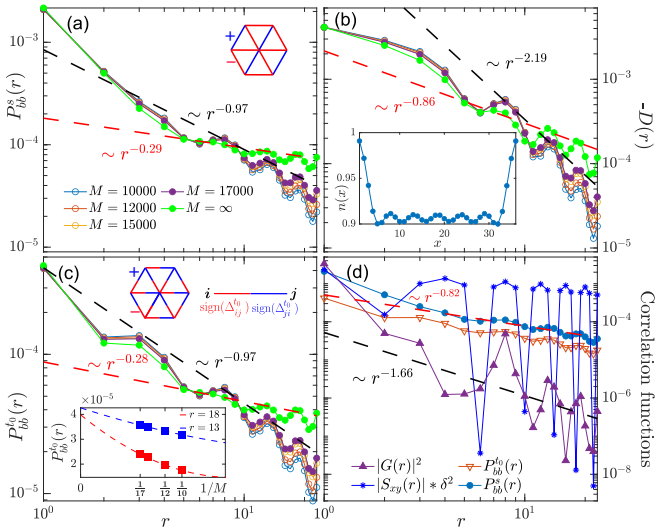

FIG. 2. Correlation functions at $\theta = \pi/12$ in the STPSC phase. (a) Scaling of the singlet pairing correlation $P^s_{bb}(r)$ through second-order polynomial extrapolation in terms of inverse bond dimension $1/M$. The extrapolated data at infinite M and $M = 17000$ are fitted by power-law decays. The inset shows the relative signs of the pairing order parameters along different bonds, which has a pattern consistent with an ordinary d-wave symmetry: sign(Δ^s_a)=sign(Δ^s_b)=−sign(Δ^s_c) [66]. (b) The density-density correlation. The inset shows the rung-averaged electron density profile $n(x) = \sum_{y=1}^{L_y}\langle\hat{n}(x,y)\rangle/L_y$ along $\boldsymbol{e}_x$, where charge stripes are observed. (c) An analogous plot for the triplet paring correlation in the opposite-spin channel $P^{t_0}_{bb}(r)$. The shown sign pattern of the pairing order parameter is consistent with an ordinary p-wave symmetry: sign($\Delta^{t_0}_a$)=sign($\Delta^{t_0}_b$)=sign($\Delta^{t_0}_c$) [66]. Each bond $\langle ij\rangle$ is divided into two halves and the half that includes $i(j)$ is denoted by the sign of $\Delta^{t_0}_{ij}(\Delta^{t_0}_{ji})$. The sign changes between the two halves because the order parameter is antisymmetric: $\Delta^{t_0}_{ij} = -\Delta^{t_0}_{ji}$. The inset shows an example of data extrapolation to $M = \infty$. (d) Comparison between different correlations at $M = 17000$ with the truncation error around 3×10^{-6}. $G(r)$ can also be fitted by an exponential decay with a correlation length around 8.7 [66].

Coexisting Singlet, Triplet and PDW SC (STPSC).— The SC order is examined by the spin-singlet and triplet pairing correlation functions $P^s_{\alpha\beta}(r)$ and $P^{t_n}_{\alpha\beta}(r)$ defined by

$$P^s_{\alpha\beta}(r) \equiv \langle\hat{\Delta}^{s,\dagger}_\alpha(\boldsymbol{r}_0)\hat{\Delta}^s_\beta(\boldsymbol{r}_0 + r\boldsymbol{e}_x)\rangle$$
$$P^{t_n}_{\alpha\beta}(r) \equiv \langle\hat{\Delta}^{t_n,\dagger}_\alpha(\boldsymbol{r}_0)\hat{\Delta}^{t_n}_\beta(\boldsymbol{r}_0 + r\boldsymbol{e}_x)\rangle, \quad (2)$$

where the reference point $\boldsymbol{r}_0 \equiv (x_0, y_0) = (L_x/4, L_y)$ and

the pairing operators $\hat{\Delta}^{s}_{\alpha}(\boldsymbol{r}_1)$ and $\hat{\Delta}^{t_n}_{\alpha}(\boldsymbol{r}_1)$ are defined on the bond along $\boldsymbol{e}_\alpha$ ($\alpha = a, b, c$) at site $\boldsymbol{r}_1$:

$$\begin{aligned}
\hat{\Delta}^{s}_{\alpha}(\boldsymbol{r}_1) &= (\hat{c}_{\boldsymbol{r}_1\uparrow}\hat{c}_{\boldsymbol{r}_1+\boldsymbol{e}_\alpha\downarrow} - \hat{c}_{\boldsymbol{r}_1\downarrow}\hat{c}_{\boldsymbol{r}_1+\boldsymbol{e}_\alpha\uparrow})/\sqrt{2} \\
\hat{\Delta}^{t_0}_{\alpha}(\boldsymbol{r}_1) &= (\hat{c}_{\boldsymbol{r}_1\uparrow}\hat{c}_{\boldsymbol{r}_1+\boldsymbol{e}_\alpha\downarrow} + \hat{c}_{\boldsymbol{r}_1\downarrow}\hat{c}_{\boldsymbol{r}_1+\boldsymbol{e}_\alpha\uparrow})/\sqrt{2} \\
\hat{\Delta}^{t_{-1}}_{\alpha}(\boldsymbol{r}_1) &= \hat{c}_{\boldsymbol{r}_1\downarrow}\hat{c}_{\boldsymbol{r}_1+\boldsymbol{e}_\alpha\downarrow}, \quad \hat{\Delta}^{t_1}_{\alpha}(\boldsymbol{r}_1) = \hat{c}_{\boldsymbol{r}_1\uparrow}\hat{c}_{\boldsymbol{r}_1+\boldsymbol{e}_\alpha\uparrow} \ .
\end{aligned} \tag{3}$$

Here $\hat{\Delta}^{t_n}_{\alpha}$ corresponds to the triplet pairing with total spin-z $S_z = n$.

Fig. 2(a) and (c) show two dominant pairing components: b-bond singlet pairing $P^{s}_{bb}(r)$ and opposite-spin-z ($S_z = 0$) triplet pairing $P^{t_0}_{bb}(r)$ for $\theta = \pi/12$ in the STPSC phase. Both exhibit power-law decay $P^{s(t_0)}_{bb}(r) \sim r^{-K^{s(t_0)}_{SC}}$ with the Luttinger exponents $K^{s(t_0)}_{SC} \approx 0.3$, suggesting strongly diverging SC susceptibilities $\chi \sim T^{-(2-K_{SC})}$ as the temperature $T \to 0$ [68]. Note also that slow power-law decays are already exhibited by the largest-M results with exponents around 0.97. The singlet pairing component is larger in amplitude than the triplet one, and they exhibit d-wave and p-wave symmetry respectively [28, 37, 69]. The mixing of singlet and triplet pairings are permitted by the absence of the inversion and spin SU(2) symmetry [70]. In particular, the absence of inversion center allows the mixing of parity-odd p-wave and parity-even d-wave basis functions in the irreducible representation E of the symmetry group C_{3v} of the system [69]. The charge density correlation function $D(r) \equiv \langle \hat{n}(\boldsymbol{r}_0)\hat{n}(\boldsymbol{r}_0 + r\boldsymbol{e}_x)\rangle - \langle \hat{n}(\boldsymbol{r}_0)\rangle\langle \hat{n}(\boldsymbol{r}_0 + r\boldsymbol{e}_x)\rangle$ in Fig. 2(b) decays algebraically with a relatively larger exponent (around 0.86), suggesting weaker charge density modulations coexisting with stronger SC. Correspondingly we observe a charge stripe order with two holes per stripe in the inset. For comparison, Fig. 2(d) presents also the in-plane spin-spin correlations $S_{xy}(r)$ defined by

$$S_{xy}(r) \equiv \langle \hat{S}^x(\boldsymbol{r}_0)\hat{S}^x(\boldsymbol{r}_0 + r\boldsymbol{e}_x) + \hat{S}^y(\boldsymbol{r}_0)\hat{S}^y(\boldsymbol{r}_0 + r\boldsymbol{e}_x)\rangle$$

and the Green's function $G(r) \equiv \sum_\sigma \langle \hat{c}^\dagger_{\boldsymbol{r}_0,\sigma}\hat{c}_{\boldsymbol{r}_0+r\boldsymbol{e}_x,\sigma}\rangle$. The in-plane spin correlation is the strongest among all correlations, characterizing a robust spin density wave order inherited from the 2D in-plane 120° Néel order at half filling based on the spin structure factor calculations [19, 40, 66]. The Green's function squared $|G(r)|^2$ is much weaker than the main pairing correlations, confirming the dominance of two-electron pairing over single-electron tunnelings.

Moreover, in the $S_z = \pm 1$ triplet pairing components, we observe quasi-long-range PDW orders with a Luttinger exponent around 0.58 in Fig. 3(a). The PDW wavevector $\boldsymbol{k}_{\rm pdw}$ can be determined by the variation of the phase of the pairing correlation under displacement along both $\boldsymbol{e_a}$ and $\boldsymbol{e_b}$. Specifically,

$$\begin{aligned}
\Phi^{n}_{bb}(x,y) \equiv& \arg\left(P^{t_n}_{bb}(x\boldsymbol{e_a} + y\boldsymbol{e_b})\right) \\
=& \arg\left(\langle \hat{\Delta}^{t_n,\dagger}_{b}(\boldsymbol{r}_0)\hat{\Delta}^{t_n}_{b}(\boldsymbol{r}_0 + x\boldsymbol{e}_a + y\boldsymbol{e}_b)\rangle\right) \\
=& \boldsymbol{k}^{\boldsymbol{n}}_{\rm pdw}\cdot(x\boldsymbol{e_a} + y\boldsymbol{e_b})
\end{aligned} \tag{4}$$

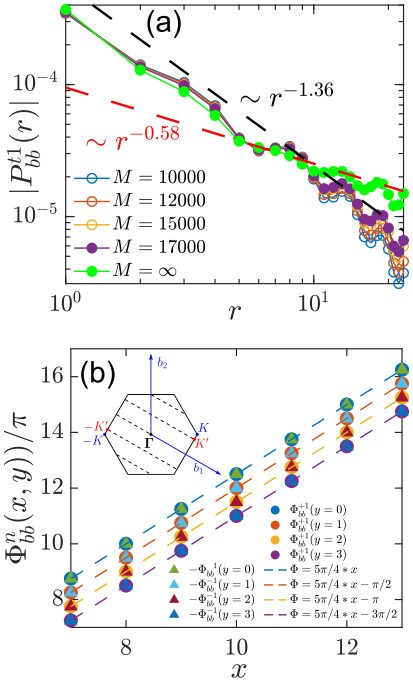

FIG. 3. PDW order for $\theta = \pi/12$ in the STPSC phase. (a) Scaling and fitting of the $S_z = 1$ component of the triplet pairing correlations. The $S_z = -1$ component is identical due to the time-reversal symmetry; (b) Characterization of spatial phase structure of PDW by $\Phi^{n}_{bb}(x,y)$. The wavevectors of PDWs are identified $\boldsymbol{k}^{+1}_{\rm pdw} = -\boldsymbol{k}^{-1}_{\rm pdw} = \boldsymbol{K'} \equiv \frac{1}{4}\boldsymbol{b_2} + \frac{5}{8}\boldsymbol{b_1}$, where $\boldsymbol{b_{1,2}}$ is the reciprocal wavevector conjugated to $\boldsymbol{e_{a,b}}$. The dashed lines in the inset denote the wavevectors in the Brillouin zone supported by the YC4 geometry.

characterizes spatial variation of the phase of the b-bond triplet pairing order parameters. In Fig. 3(b), $\boldsymbol{k}^{\pm 1}_{\rm pdw}$ is determined to be $\pm\boldsymbol{K'}$, which are the nearest accessible wavevectors to the Brillouin zone corners $\pm\boldsymbol{K}$ in the YC4 geometry. The same PDW wavevectors are identified for a- and c-bond. Note that a PDW ground state with $\boldsymbol{k}^{\pm 1}_{\rm pdw} = \mp\boldsymbol{K}$ was also predicted for the Moiré Hubbard model at $\theta = \pi/3$ by perturbative renormalization group analysis in the weak coupling regime [43, 57].

Ferromagnetic Triplet SC (FMTSC).—In the FMTSC phase, we find the dominant pairing channel to be a p-wave spin triplet. In Fig. 4(a) and (c), both $P^{t_0}_{aa}$ and $P^{t_1}_{aa}$ are non-oscillatory, in accordance with uniform SC order in the bulk of the system, and decay algebraically with exponents slightly larger than 2. An accompanying CDW order is confirmed in Fig. 4(c) by both the quasi-long-range density correlation ($\sim r^{-1.75}$) and charge stripes in the electron density profile (one hole per stripe). In Fig. 4(d), a robust in-plane ferromagnetic spin correlation is observed in reminiscence of the parent ferromagnetic order [19, 40], with the total spin $S \approx \sqrt{\langle \hat{S}^2\rangle} \approx 0.326 N_e$. The singlet paring is shown

much weaker than the triplet ones as the triplet pairing is favored by ferromagnetism. The opposite-spin-z triplet pairing correlation $P^{t_0}_{aa}$ has stronger amplitude and slower decay rate than those of the same-spin-z component $P^{t_1}_{aa}$ because the ferromagnetic order is in-plane.

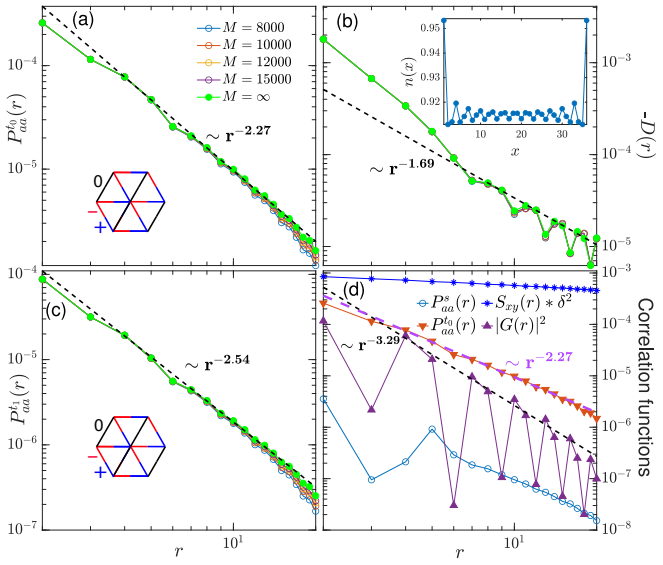

FIG. 4. Correlation functions for $\theta = 7\pi/12$ in the FMTSC phase, which is conjugated to $\theta = \pi/12$. (a) The spatial decay of $P^{t_0}_{aa}$, which is the strongest opposite-spin triplet pairing correlation among different bonds. The sign structure of the pairing order parameter is consistent with p-wave symmetry: sign($\Delta^{t_0}_a$)=-sign($\Delta^{t_0}_c$), $\Delta^{t_0}_b$=0 [66]. The black color denotes a vanishing amplitude. (b) Power-law decay of the charge-density correlation. The inset shows electron density along the axial direction, displaying a charge stripe order. (c) An analogous plot for the $S_z = 1$ component of the triplet pairing correlation P^{t1}_{aa}. (d) Comparison between different correlation functions from data at $M = 15000$ with the truncation error around 2×10^{-7}. $G(r)$ also fits an exponential decay with a correlation length around 5.4 [66].

Discussion and Summary—The FMTSC and STPSC phases are related by a spin-flip operation followed by a local gauge transformation [42] as demonstrated in the SM. Particularly, the uniform z-spin-polarized triplet pairing order at θ in the FMTSC region is conjugated to the PDW order with $\boldsymbol{k}^{\pm\mathbf{1}}_{\mathrm{pdw}} = \pm\boldsymbol{K}$ at $(2\pi/3 - \theta)$ in the STPSC region:

$$\Delta^{-\sigma,-\sigma}_{\alpha}(\frac{2\pi}{3} - \theta, \boldsymbol{r}) = e^{-i\sigma\boldsymbol{K}\cdot\boldsymbol{r} - i\sigma\beta_\alpha}\Delta^{\sigma\sigma}_{\alpha}(\theta), \qquad (5)$$

with $\beta_\alpha = \boldsymbol{e_\alpha} \cdot (\boldsymbol{b_1} - \boldsymbol{b_2})/3$, where $\boldsymbol{b_{1,2}}$ are the reciprocal wavevectors conjugated to $\boldsymbol{e_a}$ and $\boldsymbol{e_b}$ respectively. This is consistent with our observations at $\theta = 7\pi/12$ (Fig. 4(c)) and its conjugated partner $\theta = \pi/12$ (Fig. 3), albeit with a different flux (y-boundary phase) into the 4-leg cylinder. Moreover,

$$\begin{aligned}\Delta^{s}_{\alpha}(2\pi/3 - \theta) &= -\cos(\beta_\alpha)\Delta^{s}_{\alpha}(\theta) - i\sin(\beta_\alpha)\Delta^{t_0}_{\alpha}(\theta)\\ \Delta^{t_0}_{\alpha}(2\pi/3 - \theta) &= \cos(\beta_\alpha)\Delta^{t_0}_{\alpha}(\theta) + i\sin(\beta_\alpha)\Delta^{s}_{\alpha}(\theta),\end{aligned} \qquad (6)$$

which means that the singlet and opposite-spin triplet pairing components are superposed to produce their counterparts in the conjugated phase. Since the singlet pairing component at $\theta = 7\pi/12$ is found negligible compared to the triplet components, and $\beta_\alpha = 2\pi/3$ ($\alpha = a, b$) or $4\pi/3$ ($\alpha = c$), one has $|\Delta^{s}_{\alpha}(\theta = \pi/12)| \approx \sqrt{3}|\Delta^{t_0}_{\alpha}(\theta = \pi/12)|$ according to Eq. 6, which explains the larger magnitude of the spin singlet pairing than that of the triplet and the same power-law exponents in Fig. 2 (a) and (c).

However, the pairing correlations at $\theta = \pi/12$ has much stronger magnitude (over one order of magnitude larger) and slower decay rate compared to those at $\theta = 7\pi/12$ ($K_{\mathrm{SC}} \approx 0.29$ vs. $K_{\mathrm{SC}} \approx 2.27$). This in addition to the difference in charge distributions (two vs. one holes per stripe) is caused by the change of the boundary condition: the periodic boundary condition at $\theta = \pi/12$

$$\hat{c}_{\boldsymbol{r}+L_y\boldsymbol{e_y},\sigma} = \hat{c}_{\boldsymbol{r}\sigma} \qquad (7)$$

turns into a twisted boundary condition [71] at $\theta = 7\pi/12$

$$\hat{c}_{\boldsymbol{r}+L_y\boldsymbol{e_y},\sigma} = \hat{c}_{\boldsymbol{r}\sigma}e^{i2\pi\sigma L_y/3} \qquad (8)$$

after the gauge transformation, corresponding to inserting a magnetic flux of $\pm 2\pi L_y/3$ through the interior of the cylinder for electrons. The spin structure factor of the 120° Néel order for $0 < \theta < \pi/3$ is peaked at $\pm\boldsymbol{K}$, which are not resolved in the 4-leg cylinder under PBC, whereas for $\pi/3 < \theta < 2\pi/3$ the system is ferromagnetic with the peak at the system-supported momentum $\boldsymbol{\Gamma}$. Therefore, the former regime is more frustrated than the latter in the YC4 geometry and this might result in stronger SC. The sensitivity of SC to boundary conditions reveal finite-size effects in our four-leg system, so we also study a different cylinder geometry XC4 [72] (Sec. H in SM) as well as a YC3 system with $N = 40 \times 3$ (Sec. F in SM). Both systems preserve the PBC under local gauge transformation and support $\boldsymbol{\Gamma}$ and $\pm\boldsymbol{K}$ in the Brillouin zone, therefore introducing no frustration. In the XC4 geometry, we again obtain the STPSC and FMTSC phases and their SC correlations now have similar amplitudes and decay with close exponents (≈ 2), consistent with Eq. 6. In the YC3 cylinder at $\theta = 7\pi/12$, the Luttinger exponents for SC ($K^{t_0}_{\mathrm{sc}} \approx 2.28$) is nearly identical to that of the YC4 cylinder ($K^{t_0}_{\mathrm{sc}} \approx 2.27$). The observation of quasi-long-range SC order at different boundary conditions, cylinder geometries and sizes is positive evidence for the existence of SC in the 2D limit [72].

In contrast with the topological SC phases reported in the mean field and perturbative renormalization group studies of the doped TMD homobilayer [42, 43] or monolayer [69, 73], both the d- and p-wave SC phases found here are topologically trivial as the nearest-neighbor pairings acquire a phase of either 0 or π after a $\pi/3$ rotation, instead of the nontrivial phases of $\pm\pi/3$ and $\pm 2\pi/3$ for $p \pm ip$ and $d \pm id$-wave topological SC phases [31, 74, 75]. Furthermore, the SC phase here is distinct from the Ising SC found in electron-doped TMD monolayers [76–79] in

that the former arises from hole doping the parent in-plane magnetic Mott insulator at strong electronic couplings whereas the latter the pinning of the electron spins in the Cooper pairs to the out-of-plane directions by the Ising spin-orbit interaction at weak electronic couplings. Finally, the $\theta = \pi/6$ case was also studied in Ref. [50], but a rather large power-law decay exponent (≈ 3.34) was found, so only weak SC was claimed there. Consistently we find that $\theta = \pi/6$ is located at the boundary of the SC region in Fig. 1, and its conjugated pair $\theta = \pi/2$ exhibits no clear signature of SC possibly because of less frustration.

In summary, we perform large-scale DMRG simulations of the Moiré t-J model on four-leg cylinders at small hole doping. By varying the spin-dependent hopping phase induced by the out-of-plane electric field, we identify two conjugated SC phases, one of which is characterized by the coexistence of singlet d-wave, triplet p-wave SC and PDW, and the other ferromagnetic triplet SC. Our study supports twisted TMDs as a highly tunable platform for realizing exotic SC phases.

Data Availability.— The ITensor DMRG code and the data for all the figures in the main text and SM can be accessed by https://github.com/cfengno1/Moire-t-J-Model.

Acknowledgments.— We thank Yuchi He for useful comments. This work was supported by the U.S. Department of Energy, Office of Basic Energy Sciences under Grant No. DE-FG02-06ER46305. ITensor library [80] is used in this work for all DMRG calculations.

[1] E. Y. Andrei, D. K. Efetov, P. Jarillo-Herrero, A. H. MacDonald, K. F. Mak, T. Senthil, E. Tutuc, A. Yazdani, and A. F. Young, Nat Rev Mater **6**, 201 (2021), number: 3 Publisher: Nature Publishing Group.

[2] L. Balents, C. R. Dean, D. K. Efetov, and A. F. Young, Nat. Phys. **16**, 725 (2020), number: 7 Publisher: Nature Publishing Group.

[3] D. M. Kennes, M. Claassen, L. Xian, A. Georges, A. J. Millis, J. Hone, C. R. Dean, D. N. Basov, A. N. Pasupathy, and A. Rubio, Nat. Phys. **17**, 155 (2021), number: 2 Publisher: Nature Publishing Group.

[4] Y. Cao, V. Fatemi, A. Demir, S. Fang, S. L. Tomarken, J. Y. Luo, J. D. Sanchez-Yamagishi, K. Watanabe, T. Taniguchi, E. Kaxiras, R. C. Ashoori, and P. Jarillo-Herrero, Nature **556**, 80 (2018), number: 7699 Publisher: Nature Publishing Group.

[5] Y. Cao, V. Fatemi, S. Fang, K. Watanabe, T. Taniguchi, E. Kaxiras, and P. Jarillo-Herrero, Nature **556**, 43 (2018), number: 7699 Publisher: Nature Publishing Group.

[6] X. Liu, Z. Hao, E. Khalaf, J. Y. Lee, Y. Ronen, H. Yoo, D. Haei Najafabadi, K. Watanabe, T. Taniguchi, A. Vishwanath, and P. Kim, Nature **583**, 221 (2020), number: 7815 Publisher: Nature Publishing Group.

[7] G. Chen, A. L. Sharpe, P. Gallagher, I. T. Rosen, E. J. Fox, L. Jiang, B. Lyu, H. Li, K. Watanabe, T. Taniguchi, J. Jung, Z. Shi, D. Goldhaber-Gordon, Y. Zhang, and F. Wang, Nature **572**, 215 (2019), number: 7768 Publisher: Nature Publishing Group.

[8] Z. Zhang, Y. Wang, K. Watanabe, T. Taniguchi, K. Ueno, E. Tutuc, and B. J. LeRoy, Nat. Phys. **16**, 1093 (2020), number: 11 Publisher: Nature Publishing Group.

[9] S. Shabani, D. Halbertal, W. Wu, M. Chen, S. Liu, J. Hone, W. Yao, D. N. Basov, X. Zhu, and A. N. Pasupathy, Nat. Phys. **17**, 720 (2021), number: 6 Publisher: Nature Publishing Group.

[10] A. Weston, Y. Zou, V. Enaldiev, A. Summerfield, N. Clark, V. Zlyomi, A. Graham, C. Yelgel, S. Magorrian, M. Zhou, J. Zultak, D. Hopkinson, A. Barinov, T. H. Bointon, A. Kretinin, N. R. Wilson, P. H. Beton, V. I. Falo, S. J. Haigh, and R. Gorbachev, Nat. Nanotechnol. **15**, 592 (2020), number: 7 Publisher: Nature Publishing Group.

[11] T. Devakul, V. Crépel, Y. Zhang, and L. Fu, Nat Commun **12**, 6730 (2021), number: 1 Publisher: Nature Publishing Group.

[12] L. An, X. Cai, D. Pei, M. Huang, Z. Wu, Z. Zhou, J. Lin, Z. Ying, Z. Ye, X. Feng, R. Gao, C. Cacho, M. Watson, Y. Chen, and N. Wang, Nanoscale Horiz. **5**, 1309 (2020), publisher: The Royal Society of Chemistry.

[13] M. H. Naik and M. Jain, Phys. Rev. Lett. **121**, 266401 (2018), publisher: American Physical Society.

[14] Y.-H. Zhang, D. N. Sheng, and A. Vishwanath, Phys. Rev. Lett. **127**, 247701 (2021).

[15] E. C. Regan, D. Wang, C. Jin, M. I. Bakti Utama, B. Gao, X. Wei, S. Zhao, W. Zhao, Z. Zhang, K. Yumigeta, M. Blei, J. D. Carlstrm, K. Watanabe, T. Taniguchi, S. Tongay, M. Crommie, A. Zettl, and F. Wang, Nature **579**, 359 (2020), number: 7799 Publisher: Nature Publishing Group.

[16] C. Schrade and L. Fu, Phys. Rev. B **100**, 035413 (2019), publisher: American Physical Society.

[17] Y. Zhang, N. F. Q. Yuan, and L. Fu, Phys. Rev. B **102**, 201115(R) (2020), publisher: American Physical Society.

[18] F. Wu, T. Lovorn, E. Tutuc, and A. H. MacDonald, Phys. Rev. Lett. **121**, 026402 (2018), publisher: American Physical Society.

[19] F. Wu, T. Lovorn, E. Tutuc, I. Martin, and A. H. MacDonald, Phys. Rev. Lett. **122**, 086402 (2019), publisher: American Physical Society.

[20] H. Pan, F. Wu, and S. Das Sarma, Phys. Rev. Res. **2**, 033087 (2020), publisher: American Physical Society.

[21] L. Wang, E.-M. Shih, A. Ghiotto, L. Xian, D. A. Rhodes, C. Tan, M. Claassen, D. M. Kennes, Y. Bai, B. Kim, K. Watanabe, T. Taniguchi, X. Zhu, J. Hone, A. Rubio, A. N. Pasupathy, and C. R. Dean, Nat. Mater. **19**, 861 (2020), number: 8 Publisher: Nature Publishing Group.

[22] T. Li, S. Jiang, L. Li, Y. Zhang, K. Kang, J. Zhu, K. Watanabe, T. Taniguchi, D. Chowdhury, L. Fu, J. Shan, and K. F. Mak, Nature **597**, 350 (2021), number: 7876 Publisher: Nature Publishing Group.

[23] A. Ghiotto, E.-M. Shih, G. S. S. G. Pereira, D. A. Rhodes, B. Kim, J. Zang, A. J. Millis, K. Watanabe, T. Taniguchi, J. C. Hone, L. Wang, C. R. Dean, and A. N. Pasupathy, Nature **597**, 345 (2021), number: 7876

Publisher: Nature Publishing Group.
[24] C. Jin, Z. Tao, T. Li, Y. Xu, Y. Tang, J. Zhu, S. Liu, K. Watanabe, T. Taniguchi, J. C. Hone, L. Fu, J. Shan, and K. F. Mak, Nat. Mater. **20**, 940 (2021), number: 7 Publisher: Nature Publishing Group.
[25] T. Li, S. Jiang, B. Shen, Y. Zhang, L. Li, Z. Tao, T. Devakul, K. Watanabe, T. Taniguchi, L. Fu, J. Shan, and K. F. Mak, Nature **600**, 641 (2021), number: 7890 Publisher: Nature Publishing Group.
[26] Y. Tang, L. Li, T. Li, Y. Xu, S. Liu, K. Barmak, K. Watanabe, T. Taniguchi, A. H. MacDonald, J. Shan, and K. F. Mak, Nature **579**, 353 (2020), number: 7799 Publisher: Nature Publishing Group.
[27] J. Wang, J. Zang, J. Cano, and A. J. Millis, Phys. Rev. Research **5**, L012005 (2023).
[28] S. Raghu, S. A. Kivelson, and D. J. Scalapino, Phys. Rev. B **81**, 224505 (2010), publisher: American Physical Society.
[29] H.-C. Jiang, npj Quantum Mater. **6**, 1 (2021), number: 1 Publisher: Nature Publishing Group.
[30] Z. Zhu and Q. Chen, Phys. Rev. B **107**, L220502 (2023), publisher: American Physical Society.
[31] Y. Huang, S.-S. Gong, and D. N. Sheng, Phys. Rev. Lett. **130**, 136003 (2023), publisher: American Physical Society.
[32] Q.-H. Wang, D.-H. Lee, and P. A. Lee, Phys. Rev. B **69**, 092504 (2004), publisher: American Physical Society.
[33] G. Baskaran, Phys. Rev. Lett. **91**, 097003 (2003), publisher: American Physical Society.
[34] O. I. Motrunich and P. A. Lee, Phys. Rev. B **69**, 214516 (2004), publisher: American Physical Society.
[35] B. Kumar and B. S. Shastry, Phys. Rev. B **68**, 104508 (2003), publisher: American Physical Society.
[36] K. S. Chen, Z. Y. Meng, U. Yu, S. Yang, M. Jarrell, and J. Moreno, Phys. Rev. B **88**, 041103(R) (2013), publisher: American Physical Society.
[37] J. Venderley and E.-A. Kim, Phys. Rev. B **100**, 060506(R) (2019), publisher: American Physical Society.
[38] Y. Gannot, Y.-F. Jiang, and S. A. Kivelson, Phys. Rev. B **102**, 115136 (2020), publisher: American Physical Society.
[39] C. Peng, Y.-F. Jiang, Y. Wang, and H.-C. Jiang, New J. Phys. **23**, 123004 (2021), publisher: IOP Publishing.
[40] J. Zang, J. Wang, J. Cano, and A. J. Millis, Phys. Rev. B **104**, 075150 (2021), publisher: American Physical Society.
[41] J. Zang, J. Wang, J. Cano, A. Georges, and A. J. Millis, Phys. Rev. X **12**, 021064 (2022), publisher: American Physical Society.
[42] B. Zhou and Y.-H. Zhang, "Chiral and nodal superconductors in t-J model with valley contrasting flux on triangular moiré lattice," (2022), arXiv:2209.10023 [cond-mat].
[43] Y.-M. Wu, Z. Wu, and H. Yao, Phys. Rev. Lett. **130**, 126001 (2023), publisher: American Physical Society.
[44] M. Bélanger, J. Fournier, and D. Sénéchal, Phys. Rev. B **106**, 235135 (2022).
[45] M. Zegrodnik and A. Biborski, Phys. Rev. B **108**, 064506 (2023).
[46] M. Qin, T. Schfer, S. Andergassen, P. Corboz, and E. Gull, Annual Review of Condensed Matter Physics **13**, 275 (2022), _eprint: https://doi.org/10.1146/annurev-conmatphys-090921-033948.
[47] S. R. White, Phys. Rev. Lett. **69**, 2863 (1992), publisher: American Physical Society.
[48] E. Stoudenmire and S. R. White, Annual Review of Condensed Matter Physics **3**, 111 (2012), _eprint: https://doi.org/10.1146/annurev-conmatphys-020911-125018.
[49] D. P. Arovas, E. Berg, S. A. Kivelson, and S. Raghu, Annual Review of Condensed Matter Physics **13**, 239 (2022), _eprint: https://doi.org/10.1146/annurev-conmatphys-031620-102024.
[50] A. Wietek, J. Wang, J. Zang, J. Cano, A. Georges, and A. Millis, Phys. Rev. Res. **4**, 043048 (2022), publisher: American Physical Society.
[51] D. Kiese, Y. He, C. Hickey, A. Rubio, and D. M. Kennes, APL Materials **10**, 031113 (2022), publisher: American Institute of Physics.
[52] S. Gong, W. Zhu, and D. N. Sheng, Phys. Rev. Lett. **127**, 097003 (2021), publisher: American Physical Society.
[53] H.-C. Jiang and S. A. Kivelson, Phys. Rev. Lett. **127**, 097002 (2021).
[54] Z. Zhu and Q. Chen, "Superconductivity in doped triangular mott insulators: the roles of parent spin backgrounds and charge kinetic energy," (2022).
[55] D. F. Agterberg, J. S. Davis, S. D. Edkins, E. Fradkin, D. J. Van Harlingen, S. A. Kivelson, P. A. Lee, L. Radzihovsky, J. M. Tranquada, and Y. Wang, Annual Review of Condensed Matter Physics **11**, 231 (2020), _eprint: https://doi.org/10.1146/annurev-conmatphys-031119-050711.
[56] E. Berg, E. Fradkin, and S. A. Kivelson, Phys. Rev. Lett. **105**, 146403 (2010), publisher: American Physical Society.
[57] Z. Wu, Y.-M. Wu, and F. Wu, Phys. Rev. B **107**, 045122 (2023).
[58] Y.-M. Wu, P. A. Nosov, A. A. Patel, and S. Raghu, Phys. Rev. Lett. **130**, 026001 (2023), publisher: American Physical Society.
[59] K. S. Huang, Z. Han, S. A. Kivelson, and H. Yao, npj Quantum Mater. **7**, 1 (2022), number: 1 Publisher: Nature Publishing Group.
[60] A. Jaefari and E. Fradkin, Phys. Rev. B **85**, 035104 (2012), publisher: American Physical Society.
[61] G. Y. Cho, J. H. Bardarson, Y.-M. Lu, and J. E. Moore, Phys. Rev. B **86**, 214514 (2012), publisher: American Physical Society.
[62] P. A. Lee, Phys. Rev. X **4**, 031017 (2014), publisher: American Physical Society.
[63] R. Soto-Garrido and E. Fradkin, Phys. Rev. B **89**, 165126 (2014), publisher: American Physical Society.
[64] J. Venderley and E.-A. Kim, Science Advances **5**, eaat4698 (2019), publisher: American Association for the Advancement of Science.
[65] D. Shaffer and L. H. Santos, Phys. Rev. B **108**, 035135 (2023).
[66] See Supplemental Material at http://link.aps.org/ supplemental/ for supporting results.
[67] S. Yan, D. A. Huse, and S. R. White, Science **332**, 1173 (2011), publisher: American Association for the Advancement of Science.
[68] E. Arrigoni, E. Fradkin, and S. A. Kivelson, Phys. Rev. B **69**, 214519 (2004), publisher: American Physical Society.
[69] Y.-T. Hsu, A. Vaezi, M. H. Fischer, and E.-A. Kim, Nat Commun **8**, 14985 (2017), number: 1 Publisher: Nature Publishing Group.
[70] S. Yip, Annual Review of Condensed Matter Physics

5, 15 (2014), _eprint: https://doi.org/10.1146/annurev-conmatphys-031113-133912.
[71] Y. Gannot and S. A. Kivelson, Phys. Rev. B **107**, 075127 (2023), publisher: American Physical Society.
[72] A. Szasz, J. Motruk, M. P. Zaletel, and J. E. Moore, Phys. Rev. X **10**, 021042 (2020), publisher: American Physical Society.
[73] N. F. Q. Yuan, K. F. Mak, and K. T. Law, Phys. Rev. Lett. **113**, 097001 (2014), publisher: American Physical Society.
[74] Y. Huang and D. N. Sheng, Phys. Rev. X **12**, 031009 (2022), publisher: American Physical Society.
[75] Y.-F. Jiang and H.-C. Jiang, Phys. Rev. Lett. **125**, 157002 (2020), publisher: American Physical Society.
[76] B. T. Zhou, N. F. Q. Yuan, H.-L. Jiang, and K. T. Law, Phys. Rev. B **93**, 180501(R) (2016), publisher: American Physical Society.
[77] J. M. Lu, O. Zheliuk, I. Leermakers, N. F. Q. Yuan, U. Zeitler, K. T. Law, and J. T. Ye, Science **350**, 1353 (2015), publisher: American Association for the Advancement of Science.
[78] X. Xi, Z. Wang, W. Zhao, J.-H. Park, K. T. Law, H. Berger, L. Forr, J. Shan, and K. F. Mak, Nature Phys **12**, 139 (2016), number: 2 Publisher: Nature Publishing Group.
[79] Y. Saito, Y. Nakamura, M. S. Bahramy, Y. Kohama, J. Ye, Y. Kasahara, Y. Nakagawa, M. Onga, M. Tokunaga, T. Nojima, Y. Yanase, and Y. Iwasa, Nature Phys **12**, 144 (2016), number: 2 Publisher: Nature Publishing Group.
[80] M. Fishman, S. White, and E. Stoudenmire, SciPost Phys. Codebases , 4 (2022).